

V

Results

This chapter presents the results obtained with the simulations and measurements explained until this point. In all cases the code's rate was varied while P_{er} was kept constant and the decoded content was evaluated with respect to degradation, by using the following mechanisms: (1) objective quality measurements, namely Blocking Artifact Measure, (2) monitoring of Transport Stream parameters and, finally, (3) subjective visual impairments.

These measurements were repeated for three types of error condition explained in [10]:

- bursts of packet erasures
- single packet erasures
- combination of burst and single packet erasures

The results are presented in the sections that follow.

V.1 LT Code Performance

This section makes an assessment of the LT code by itself — the variation of the degradation of the decoded content when the code rate is varied was observed. The measured degradation in this situation examines the probability of unrecovered symbols in the decoded content. We have also run an experiment which enabled us to verify the universality property of LT-codes.

(a) LT Code Performance: probability of unrecovered symbols

The code's rate is varied within a range that allows us to observe the transition from a very good quality decoded content, down to a very impaired decoded content, while the channel erasure probability P_{er} is kept constant at 0.03.

Fig. V.1 shows the resulting performance for an LT code with dimension $k = 7,896$ bytes. It can be noted that very little decoding is possible until approximately $n = 1.08.k$, i.e., for $n = 8,528$ bytes, given P_{er} , at which point, a behavior similar to a *decoding waterfall* is observed.

This simulation was repeated for the three channel erasure patterns mentioned and no significant variation in the degradation was observed.

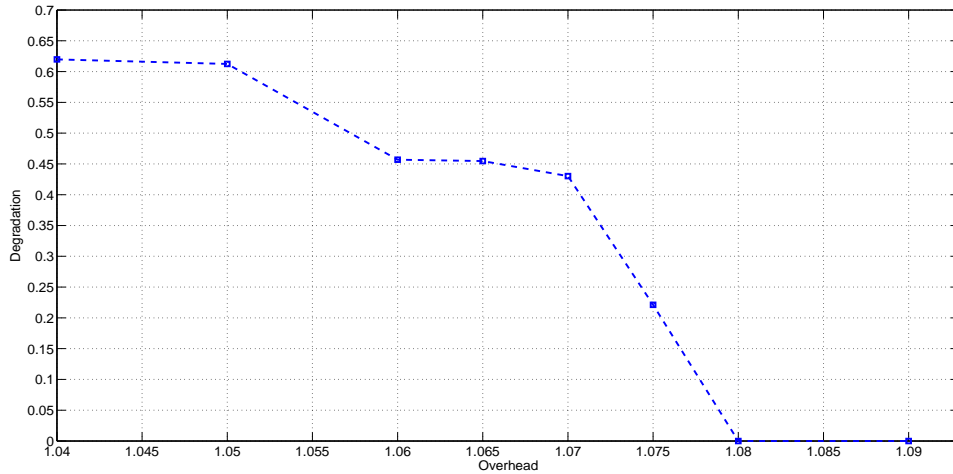


Figure V.1: LT Code performance

(b) Universality property

The second aspect verified in this section concerns the *Universality Property*, more specifically the characteristic of Fountain codes, that subsets of the same size, of symbols belonging to the same encoding symbols block, will be equally useful in the decoding process. More detailed explanation regarding the Universality Property of Fountain codes can be found in the Appendix A.

In order to evaluate this property, an encoding symbols block of size N is generated and a subset of n randomly chosen encoding symbols is generated, being $n < N$. These symbols and the associated connections are provided to the LT decoder. The *recovered symbols to source symbols* ratio, referred herein as *decode-ability*, is computed. This experiment is repeated multiple times for the same encoding symbols block and the result is shown in the histograms of figures VI.2 and VI.3, for $n = 8,211$ and $n = 8,370$, respectively. In both cases the erasure rate P_{er} was kept constant at 0.03.

For the $LT[8211,7896]$, the decode-ability varies from 0.31 to 0.33, whereas the $LT[8370,7896]$ presents values between 0.74 and 0.79. These histograms indicate that decode-ability is more or less the same for subsets of same size, but distinct elements of a larger encoded symbols block generated in the same LT process.

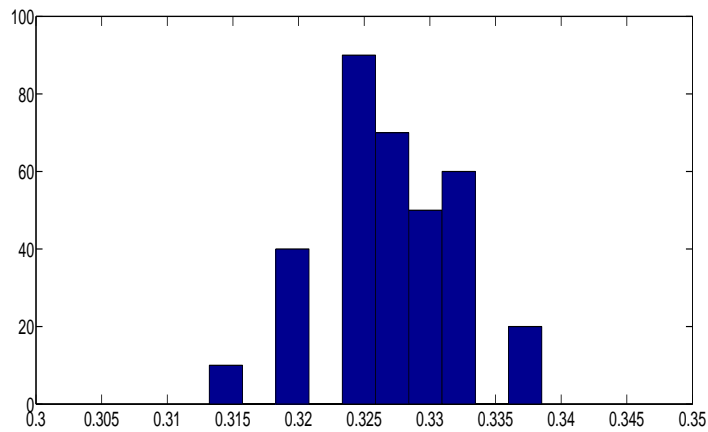


Figure V.2: Decode-ability Histogram for $LT[8211,7896]$

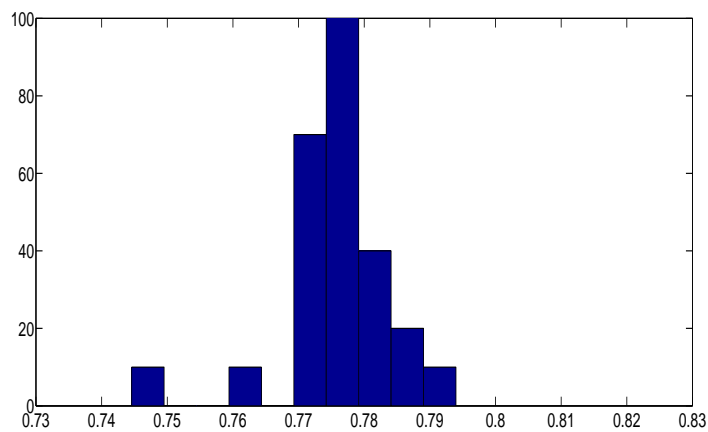


Figure V.3: Decode-ability Histogram for $LT[8370,7896]$

V.2 Comparing the Performance of RS and LT codes

The results presented herein are associated to the simulation scenarios explained in chapter IV. The results were divided in three subsections, as per erasure pattern employed in the channel simulation. Differently from the

Reed-Solomon codes, the LT code did not present any significant performance variation when the distinct erasure patterns were used.

(a) Random burst erasures

Figure V.4 shows the performance results for both Reed-Solomon schemes and the LT coding scheme. The Reed-Solomon codes present a much better performance until a value of $N \approx 1.08 \cdot k$, at which point, any new LT encoded symbol that arrives successfully at the LT decoder, contributes significantly with the LT decoding process and the same outperforms the Reed-Solomon Schemes.

Another interesting aspect, is that the second dimension of Reed-Solomon does not provide improvement for the *burst-only* erasure pattern. Actually, it increases the overhead at no significant benefit, decreasing performance measured against overhead cost, making the single dimensional Reed-Solomon advantageous for this type of erasure pattern.

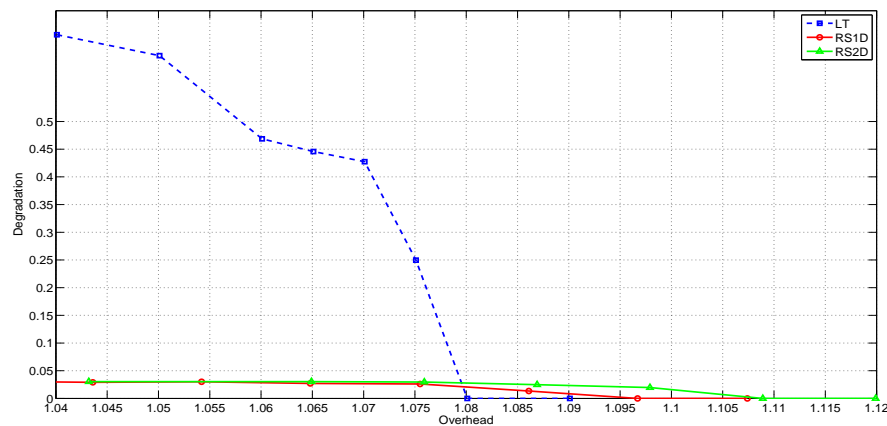


Figure V.4: Performance Comparison for random burst packet erasure

(b) Random single packet erasures

In this case, the two dimensional and the single-dimensional Reed-Solomon schemes present very similar performances, as shown in figure V.5.

(c) Combination of Random single packet erasures and random burst erasures

This erasure pattern is said to be more realistic according to [10]. In the channel simulation herein, approximately half of the erasures are distributed

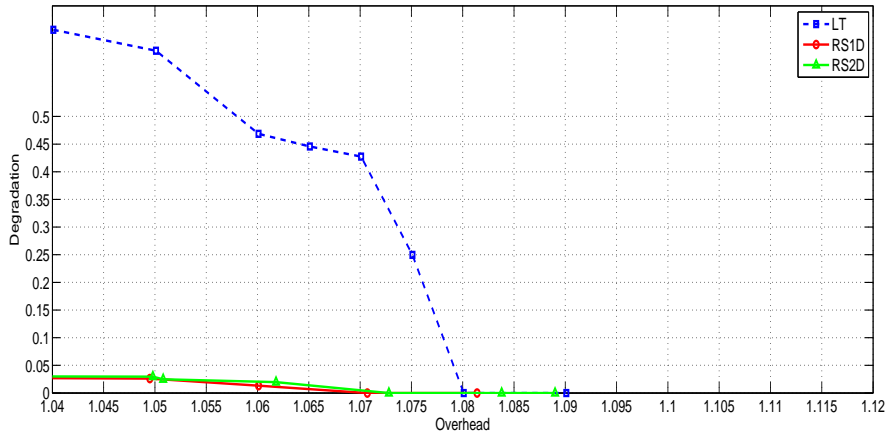


Figure V.5: Performance Comparison for random single packet erasures

as single packet erasures, whereas the other half as bursts of 7 packets being erased.

It can be noted that in this case the second dimension for the Reed-Solomon scheme provides an improvement over the single-dimensional one. The LT scheme still outperforms the Reed-Solomon schemes at $n \approx 1.08$.

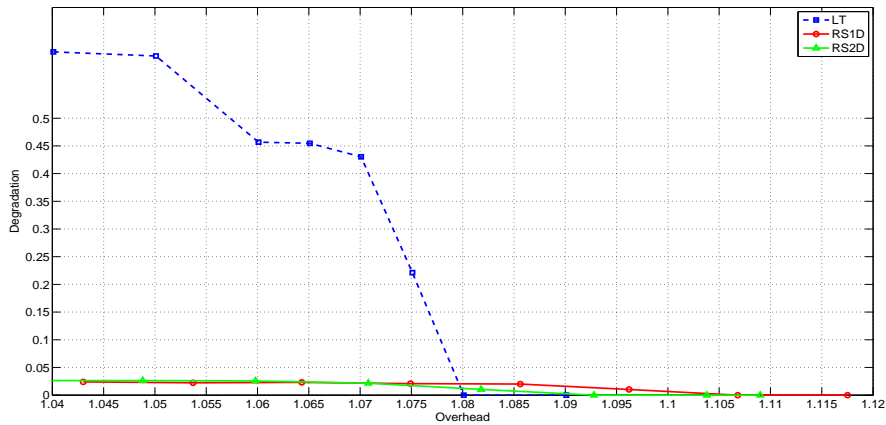


Figure V.6: Performance Comparison for random burst and single packet erasures

V.3 Visual impairments

This section intends to show the visual impairment observed in particular frames of the decoded video image. A sample frame of the decoded content resulting from the LT process is shown in figure V.7. This snapshot was taken from an LT decoded content recovered from the channel presented

in the previous sub-section, which combines punctual erasures with bursts of packets being erased. From the performance curves obtained previously, no degradation is monitored at this point and thus, no visual impairments are observed in the snapshot.

Figures V.8 and V.9 show snapshots of samples resulting from the single and two-dimensional Reed-Solomon processes respectively, when submitted through the same channel with combined patterns and erasure probability P_{err} , as with the LT scheme.



Figure V.7: Visual impairments for LT at $N \approx 0.8k$



Figure V.8: Visual impairments for RS1D at $N \approx 0.8k$



Figure V.9: Visual impairments for RS2D at $N \approx 0.8k$

V.4 Blocking Artifact Measure

The Blocking Artifact Measure employed herein is based in [12]. This is a non-referencing measurement method, i.e., it does not require a known reference at the measurement point. The result is an index calculated per frame, that is proportional to the discontinuities present in the frame.

In practical monitoring applications, the user defines a threshold that suits his needs and a monitoring platform may trigger an alarm, whenever this threshold is trespassed.

Such method is implemented in electronic monitoring that intends to replicate as close as possible the results of standardized subjective quality evaluation, for instance, defined in [18] and [19]. These methods consist of a viewer's opinion on the quality of the video sequence perceived by him or her. Replacing such methods with electronic monitoring will save considerable time and human resources.

Nevertheless, a few challenges have to be overcome by objective analysis of multi-media content. The first is associated to architectural characteristics of most transmission and distribution networks, which do not provide access to the bit stream. As such, methods that do not require referencing, i.e. are based in the incoming content subject to analysis, have to be implemented. The second important challenge is to distinguish block discontinuities from natural contours of the image. This is critical for discontinuity correction algorithms. The most efficient correction algorithms to date are based on low-pass filtering and this might undesirably affect natural contours of the image instead of unwanted discontinuities.

In the Blocking Artifact Measure method explained in [12], a variable denominated $D_{H,norm}$ is the ratio of the absolute normalized gradient and the average gradient calculated over N pixels to the right and to the left. $D_{H,norm}$ is then summed across all lines and the value S_H is obtained for quantifying the blocking grid discontinuity per pixel position across all lines. Usually, the result will contain outstanding peaks in the pixel positions where block edges result from the *DCT* source coding schemes, i.e. every 8 pixels in an MPEG-2 coded content. Finally, the Blocking Strength BS is given by the ratio between the average of S_H measured in the edge position and the intermediate pixels.

$$D_{H,norm}(i, j) = \frac{|I(i+1, j) - I(i, j)|}{1/2N \sum_{-N \dots N, n \neq 0} |I(i+n+1, j) - I(i+n, j)|}$$

$$S_H(i) = \sum_{j=1}^{nl} D_{H,norm}(i, j)$$

$$BS = \frac{\bar{S}_H(block)}{\bar{S}_H(non - block)}$$

Figure V.10 shows a frame with high rate of discontinuity. The sum of the discontinuities across all lines for this frame is shown in figure V.11. The spikes indicating the positions of higher discontinuities can provide information on the grid size employed in the source coding process and drive a low-pass filter for correction of these unwanted discontinuities. For the sake of comparison, figures V.12 and V.13 show a frame with lower discontinuity rate and its associated result, respectively. It can be noted that, in this case the spikes have much lower pronunciation against neighboring positions.

Finally, an index, that is proportional to the sum of discontinuities in each frame, was calculated for the decoded video sequences resulting from the simulations with LT and both Reed-Solomon schemes, when the combined erasure pattern with error probability $P_{err} \approx 0.03$ was employed. The result for sequences of 10 frames of each sample is shown in figure V.14.



Figure V.10: Sample frame 'A' with high rate of discontinuity

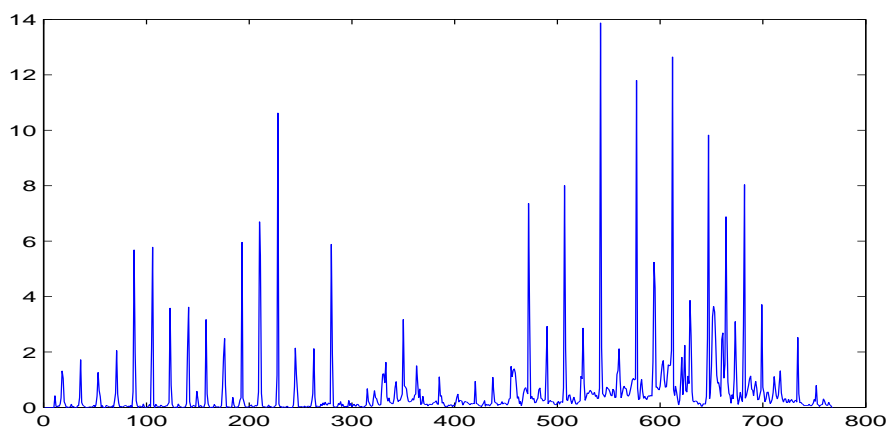


Figure V.11: Sum of discontinuities across all lines of frame 'A'



Figure V.12: Sample frame 'B' with low rate of discontinuity

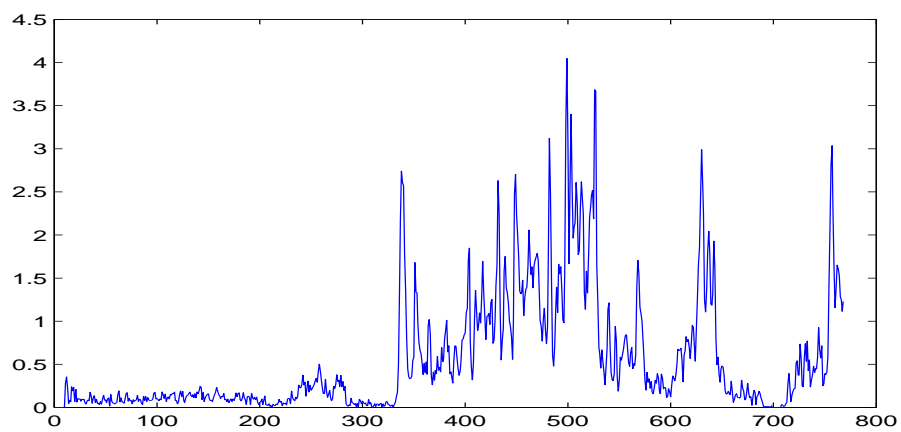


Figure V.13: Sum of discontinuities across all lines of frame 'B'

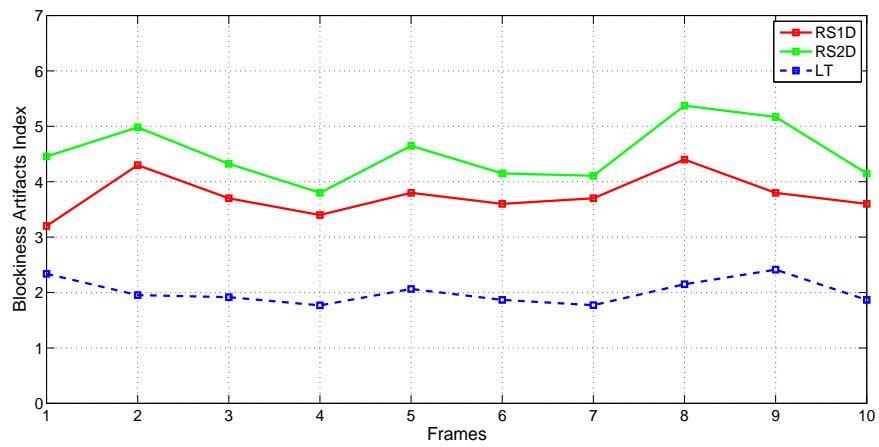


Figure V.14: BAI measurements

